# Early recombination as a solution to the $H_0$ tension

Toyokazu Sekiguchi [1,*] and Tomo Takahashi [2,†]

[1] *Theory Center, IPNS, KEK, Tsukuba 305-0801, Japan*

[2] *Department of Physics, Saga University, Saga 840-8502, Japan*

(Received 15 July 2020; revised 22 January 2021; accepted 17 March 2021; published 12 April 2021)

We show that the $H_0$ tension can be resolved by making recombination occur earlier, keeping the fit to cosmic microwave background (CMB) data almost intact. We provide a suite of general necessary conditions to give a good fit to CMB data while realizing a high value of $H_0$ suggested by local measurements. As a concrete example for a successful scenario with early recombination, we demonstrate that a model with a time-varying $m_e$ can indeed satisfy all of the conditions. We further show that such a model can also be well fitted to low-$z$ distance measurements of baryon acoustic oscillations (BAO) and type Ia supernovae (SNeIa) with a simple extension of the model. A time-varying $m_e$ in the framework of $\Omega_k\Lambda$CDM is found to be a sufficient and excellent example of a solution to the $H_0$ tension, yielding $H_0 = 72.3^{+2.7}_{-2.8}$ km/sec/Mpc from the combination of CMB, BAO, and SNeIa data *even without* incorporating any direct local $H_0$ measurements. Employing the Bayesian posterior predictive distribution, we find that this model can reduce the $H_0$ tension in the reference $\Lambda$CDM model from $4.8\sigma$ down to $2.2\sigma$. Apart from the $H_0$ tension, this model is also favored from the viewpoint of the CMB lensing anomaly.

DOI: 10.1103/PhysRevD.103.083507

## I. INTRODUCTION

The Hubble constant $H_0$ is one of the most relevant cosmological parameters characterizing the Universe. It has long been studied by the distance ladder, which now utilizes Cepheids and type Ia supernovae (SNeIa) as standard candles [1]. Meanwhile, many other means have been devised. For instance, gravitational lens time delay measurements now rival the distance ladder in local (almost direct) measurements of $H_0$ [2]. Moreover, the cosmic microwave background (CMB) and baryon acoustic oscillations (BAO) allow us to measure cosmic distances to very different redshifts ($z \simeq 10^3$ and $z \lesssim 2$) based on the scales of the sound horizon of the photon-baryon fluid $r_s$ at recombination ($z = z_*$) and the drag epoch ($z = z_{\rm drag}$), respectively. Consistency in the cosmic expansion history over such a huge range of redshifts enables us to infer $H_0$.

However, as measurements of $H_0$ become more precise, disagreements become apparent between local direct measurements and other indirect ones such as CMB. The value of $H_0$ from local measurements, $H_0 = (73.8 \pm 1.0)$ km/sec/Mpc [3], is about 10% larger than that from CMB, $H_0 = (67.36 \pm 0.54)$ km/sec/Mpc [4], assuming the canonical flat $\Lambda$CDM ($\Lambda$CDM hereafter) model. The significance of the $H_0$ tension is now more than $5\sigma$. Interestingly, different and independent measurements appear consistent within either local or indirect measurements (For a recent review, see Ref. [3]). This indicates that a single systematic error alone cannot remove the tension.

A number of cosmological solutions have been proposed already. However, it seems extremely difficult to solve the tension when one combines various observations such as CMB, BAO, and SNeIa. The reason for the difficulty has been clarified in Refs. [5–9]. SNeIa and distance ladder jointly measure luminosity distance seamlessly at $z \lesssim 2$. This gives the transverse distance $D_M(z)$ at the redshifts of BAO measurements, where $D_M(z)$ is given by

$$D_M(z) = \begin{cases} \frac{\sin[\sqrt{-\Omega_k}H_0\chi(z)]}{\sqrt{-\Omega_k}H_0} & \text{for } \Omega_k < 0 \text{ (closed)}, \\ \chi(z) & \text{for } \Omega_k = 0 \text{ (flat)}, \\ \frac{\sinh[\sqrt{\Omega_k}H_0\chi(z)]}{\sqrt{\Omega_k}H_0} & \text{for } \Omega_k > 0 \text{ (open)}, \end{cases} \tag{1}$$

with $\chi(z) = \int_0^z \frac{dz}{H(z)}$ being the comoving distance to $z$. This enables a model-independent estimation of $r_s(z_{\rm drag})$. Enhancing $H_0$ by 10% requires decreasing $r_s(z_*) \propto r_s(z_{\rm drag})$ by the same rate,[1] which is very difficult while keeping a reasonable fit to CMB. This also explains why models modifying only late-time expansion can increase $H_0$ only marginally.

[1] Given the baryon drag at $z_*$, $R(z_*) = 3\rho_b(z_*)/4\rho_\gamma(z_*)$, which is very precisely determined by CMB power spectra, specifying either $r_s(z_*)$ or $r_s(z_{\rm drag})$ virtually determines the other.

*tsekiguc@post.kek.jp
†tomot@cc.saga-u.ac.jp

 

The considerations above lead to the following four necessary conditions which successful cosmological solutions to the $H_0$ tension should satisfy:

(1) In order not to spoil the successful fit achieved by $\Lambda$CDM, CMB power spectra should be left almost intact except at low $\ell$, where cosmic variance is large.
(2) $r_s(z_*) \propto r_s(z_{\rm drag})$ is reduced by $\simeq 10\%$.
(3) $D_M(z_*)$ is reduced, so that $\theta_s(z_*) = r_s(z_*)/D_M(z_*)$ is kept constant (this is somewhat redundant with condition 1).
(4) BAO, SNeIa, and other low-$z$ distance measurements should also be fitted well.

With the first condition being met, the second condition is quite difficult to be satisfied. Many attempts have been made to increase the expansion rate by, e.g., adding extra energy components (see Ref. [9] for review). However, these modifications have some limitations since the relative scale between the sound horizon and the Silk scale, or the photon diffusion length, also varies, which inevitably violates the first condition [9]. This is the reason why those attempts can only partially mitigate the $H_0$ tension.

In this paper we pursue a cosmological solution to the $H_0$ tension, in particular focusing on modified recombination (see the earlier studies in Refs. [10,11] for general discussion but without concrete models). We first argue how one can modify the recombination epoch while keeping CMB power spectra almost unchanged. Then, as a working example we discuss a model with a time-varying electron mass $m_e$ (for possible models of time-varying $m_e$, see, e.g., Refs. [12,13] and the recent review Ref. [14]),[2] which can sizably shift $z_*$ and $z_{\rm drag}$ from the baseline model without affecting CMB power spectra much.[3]

In the following, we often refer to the *Planck* 2018 best-fit $\Lambda$CDM model [4] as the baseline. The reduced Hubble constant and density parameters are given by $h = H_0[100\ \mathrm{km/sec/Mpc}]$ and, e.g., $\omega_i = \Omega_i h^2$ for component $i$, respectively. Let $\Delta_x$ denote the fractional variation in a quantity $x$ from the baseline value [e.g., $\Delta_{m_e} = \log(m_e/m_{e,\rm baseline})$].

## II. EFFECTS OF EARLY RECOMBINATION ON CMB

Let us discuss the effects of early recombination on the CMB and how to cancel those effects by varying cosmological parameters. In the analytical argument below, we utilize the scale factor at recombination $a = a_*$, which is useful since it can well capture effects of modified recombination on the CMB.

CMB observations tightly constrain the following two quantities at the recombination $a = a_*$:

$$R(x) = \frac{3\omega_b a_*}{4\omega_\gamma} x, \tag{2}$$

$$[a^2 H](x) = \frac{1}{L}\sqrt{\omega_m a_* x + \omega_r}, \tag{3}$$

where $x \equiv a/a_*$ is the scale factor normalized to unity at recombination and $L = (H_0/h)^{-1} \simeq 2998$ Mpc is a constant length. The former gives the baryon drag, which is measured by the relative heights of even and odd acoustic peaks. The latter determines the early integrated Sachs-Wolfe (ISW) effect, which is measured by the heights of acoustic peaks relative to the SW plateau. From Eqs. (2) and (3), we can leave both $R$ and $a^2 H$ unaffected as functions of $x$ by varying $\omega_b$ and $\omega_m$ inversely proportionally to $a_*$:

$$\Delta_{\omega_b} = \Delta_{\omega_m} = -\Delta_{a_*}. \tag{4}$$

Now we consider the sound horizon at the recombination epoch,

$$r_s(z_*) = \frac{a_*}{\sqrt{3}} \int_0^1 \frac{1}{\sqrt{1 + R(x)}} \frac{dx}{[a^2 H](x)}, \tag{5}$$

from which we can immediately see that $r_s(z_*) \propto a_*$ when we vary $\omega_b$ and $\omega_m$ in accord with Eq. (4) (i.e., $R$ and $a^2 H$ remain unchanged as functions of $x$). In order to not change CMB power spectra, the relative scale of the Silk scale $1/k_{D*}$ to $r_{s*}$ should be kept unchanged, where

$$\frac{1}{k_D(z_*)^2} = \frac{a_*^2}{6} \int_0^1 \frac{R^2 + \frac{16}{15}(1+R)}{(1+R)^2} \frac{1}{a_*^2 n_e \sigma_T} \frac{dx/x}{[a^2 H]}. \tag{6}$$

This requires

$$1/k_D(z_*) \propto a_*. \tag{7}$$

Finally, the viewing angle of the sound horizon, $r_s(z_*)/D_M(z_*)$, should be kept constant, which means that $D_M(z_*)$ should vary proportionally to $a_*$. Within the $\Lambda$CDM background, we find that

$$\Delta_h \approx -3.23 \Delta_{a_*} \tag{8}$$

approximately realizes $D_M(z_*) \propto a_*$, where the numerical coefficient is evaluated around the baseline.

Conditions (4) and (8) can be easily satisfied by varying standard cosmological parameters. In contrast, Eq. (7) is nontrivial. As we will show below, varying $m_e$ models can satisfy this nontrivial condition as well as other ones.

## III. VARYING $m_e$ AND CMB POWER SPECTRA

As a working example, here we consider a model with a time-varying $m_e$. The electron mass $m_e$ affects the physics

[2] In the following discussion, we assume a different value of $m_e$ for the present time and the recombination epoch. In this sense, $m_e$ is time-varying; however, we make a simplified assumption where $m_e$ is constant until some time after recombination, and then at some epoch $m_e$ takes the present value.

[3] The possible role of a varying $m_e$ in the $H_0$ tension was pointed out in Ref. [15].

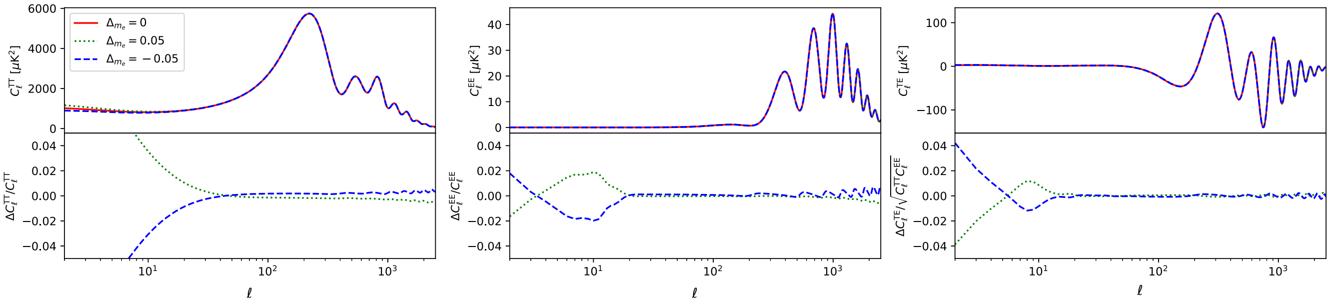

FIG. 1. CMB power spectra with $\Delta_{m_e} = 0, \pm 0.05$ in the ΛCDM background along the parameter directions (4), (8), and (9).

of CMB at recombination in the following ways (see Refs. [16,17] for a detailed discussion).

(1) Energy levels of hydrogen: $E \propto m_e$.
(2) Thomson scattering cross section: $\sigma_\mathrm{T} \propto m_e^{-2}$.
(3) Others (two-photon decay rate, photoionization cross section, recombination coefficients, etc.).

If recombination proceeds in thermal equilibrium, the third set of effects can be omitted. Although nonequilibrium processes are evident in observed CMB power spectra, their impact is indeed relatively minor as long as $m_e$ alone is varied [16]. Neglecting the third set of effects to simplify our discussion, $a_*$ is inversely proportional to $m_e$ through the first effect:

$$\Delta_{m_e} = \Delta_{T_\gamma(z_*)} = -\Delta_{a_*}. \tag{9}$$

To see how $1/k_D$ in Eq. (6) is modified in response to $m_e$, let us consider the following factor:

$$a_*^2 n_e \sigma_T = x_e \frac{1 - Y_p}{m_H} \frac{\rho_\mathrm{crit}}{h^2} (\omega_b a_*) \left( \frac{\sigma_T}{a_*^2} \right) \frac{1}{x^3}, \tag{10}$$

where $x_e$, $Y_p$, $m_H$, and $\rho_\mathrm{crit} = \frac{3h^2}{8\pi L^2 G}$ are the ionization fraction, mass fraction of $^4$He, hydrogen mass, and critical density, respectively. When we vary $\omega_b$ according to Eq. (4), Eq. (10) does not change as a function of $x$.[4] Thus, the integral in Eq. (6) is kept constant, which means that $1/k_D(a_*) \propto a_*$ and Eq. (7) is satisfied.

Figure 1 demonstrates the parameter degeneracy in CMB power spectra, which are computed using CAMB [18] with the recombination code HyRec [19], with effects of varying $m_e$ being incorporated in full. Here we vary $m_e$ by $\pm 5\%$ with $\omega_b$, $\omega_m$, and $h$ being varied simultaneously according to Eqs. (4) and (8). Except for low-$\ell$ in $C_\ell^{TT}$, where the late-ISW effect is significant, CMB power spectra remain remarkably unchanged. One can also find that the parameter degeneracy in Eqs. (4) and (8) is apparent in parameter estimation based on CMB alone in previous works [15–17]. These show that varying $m_e$ satisfies the first three conditions we raised in the Introduction.

## IV. LOW-$z$ DISTANCES

While CMB spectra are almost conserved, the parameter modifications (4) and (8) in general also modify late-time expansion and geometric distances, which are severely constrained by BAO and SNeIa data. To see this, we plot the late-time distance and the expansion history in Fig. 2. Here we have introduced two quantities,

$$\theta_T(z) \equiv \frac{r_s(z_\mathrm{drag})}{D_M(z)}, \qquad \theta_L(z) \equiv r_s(z_\mathrm{drag}) H(z), \tag{11}$$

which are nothing but the scales of BAO measured along the transverse and line-of-sight directions, respectively.[5] In addition, BAO measurements from the 6dF Galaxy Survey [20] at the effective redshift $z_\mathrm{eff} = 0.106$, the SDSS DR7 main Galaxy samples [21] $z_\mathrm{eff} = 0.15$, and the SDSS DR12 galaxy samples [22] $z_\mathrm{eff} = 0.38, 0.51, 0.61$ as well as SNeIa data [23] are overlaid in the same figure for reference.[6]

When the ΛCDM background is assumed (left panel of Fig. 2), the model effectively becomes a one-parameter model according to Eqs. (4) and (8). One can see that the late-time geometry changes as $m_e$ varies from the baseline. Therefore, low-$z$ distance measurements such as BAO or SNeIa in combination with CMB can tightly constrain $m_e$ since the parameter degeneracy is lifted.

In the ΛCDM background, there are no more degrees of freedom to tune the late-time geometry while $\Delta_{m_e}$ is kept nonzero, and hence it is impossible to solve the $H_0$ tension with just a varying $m_e$. However, it easily becomes possible when the background model is extended appropriately. In the right panel of Fig. 2, the background cosmology is extended

[4] If we neglect the nonequilibrium nature of recombination, $x_e$ does not change as a function of $x$. We have also omitted the marginal dependence of $Y_p$ on $\omega_b$ in the big bang nucleosynthesis prediction.

[5] Precisely speaking, $\theta_L(z)$ is the separation of the BAO scale along the line of sight in $z$.

[6] The BAO data at $z_\mathrm{eff} = 1.06$ and 1.5 originally given in terms of $\theta_V(z) = [z\theta_T(z)^2\theta_L(z)]^{1/3}$ are interpreted as constraints on $\theta_T(z)$, since $\theta_V \approx \theta_T$ at $z \ll 1$. We have normalized the SNeIa luminosity distances to give a $D_M(z)$ consistent with BAO at $z \simeq 0.5$.

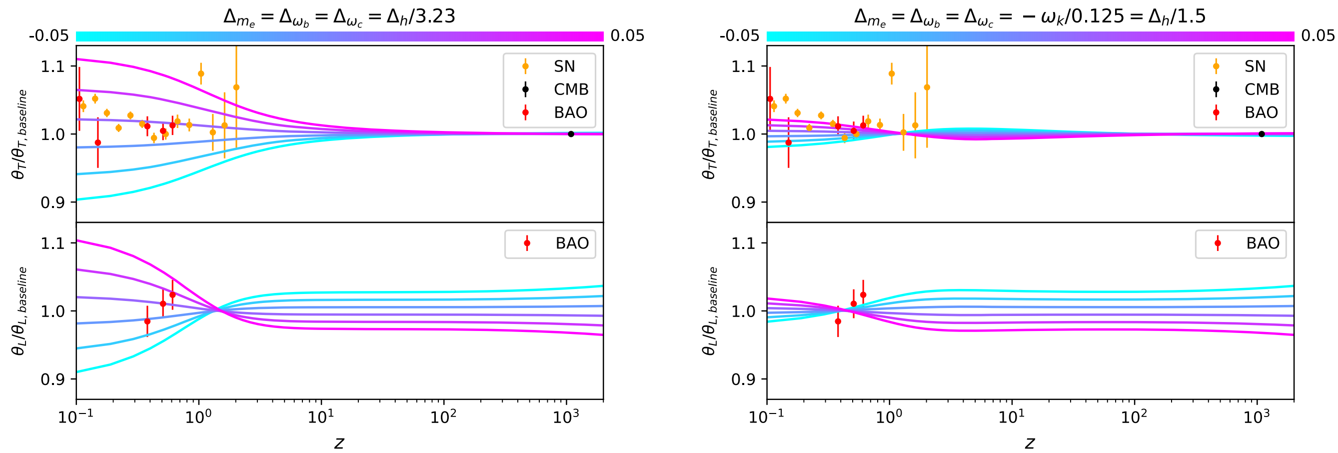


FIG. 2. Left: transverse $\theta_T(z)$ (upper) and longitudinal $\theta_L(z)$ (lower) BAO separations in varying $m_e$ with the ΛCDM background. The color bar indicates the value of $\Delta_{m_e} \in \{-0.05, -0.03, -0.01, 0.01, 0.03, 0.05\}$ that each line has. The other cosmological parameters $(\omega_b, \omega_c, h)$ are varied with $m_e$ in accordance with Eqs. (4), (8), and (9). CMB, BAO, and (normalized) SNeIa data are also plotted. Right: same as in the left panel but with the $\Omega_k$ΛCDM background, with Eq. (8) being replaced by Eq. (12).

to allow a nonflat Universe ($\Omega_k$ΛCDM hereafter) and we plot the late-time geometry along a parameter direction

$$\Delta_h = 1.5\Delta_{m_e}, \qquad \omega_k = -0.125\Delta_{m_e} \tag{12}$$

instead of Eq. (8). This realizes a good fit to the low-$z$ distance observations even with $\Delta_{m_e}$ as large as 5%. The curvature of the Universe plays an essential role here. As can be read from Eq. (1), deviations from flatness grow as $\chi(z)\sqrt{|\omega_k|}/L$ increases. Therefore, the curvature selectively affects only the angular diameter distance to CMB and offers the freedom for low-$z$ and CMB distances to be fitted well simultaneously even with large $\Delta_{m_e}$. Therefore, all four conditions in the Introduction are satisfied in the $\Omega_k$ΛCDM background with a varying $m_e$.

## V. MCMC PARAMETER ESTIMATION

We perform a Markov chain Monte Carlo (MCMC) analysis using CosmoMC [24] modified to incorporate a varying $m_e$. We adopt the *Planck* 2018 reference CMB likelihood TT, TE, EE + lowE [25] in combination with the BAO [20–22] and SNeIa data [23]. To verify our results, we have checked the consistency with Ref. [15], where CosmoRec [26] was used for the recombination calculation, in a ΛCDM background by adopting the same CMB and BAO data.

Figure 3 shows the posterior distribution of $H_0$ in models with a varying $m_e$ in different backgrounds, including ΛCDM, $\Omega_k$ΛCDM, and $w$CDM, where the dark energy (DE) equation of state (EoS) $w$ is assumed to be constant, and $ww_a$CDM models, where the DE EoS is parametrized as in Refs. [27,28]. For reference, the ΛCDM model without a varying $m_e$ ("reference" model hereafter) is also plotted. We also compare those posterior distributions with the direct measurement $H_0 = 74.1 \pm 1.3$ km/sec/Mpc

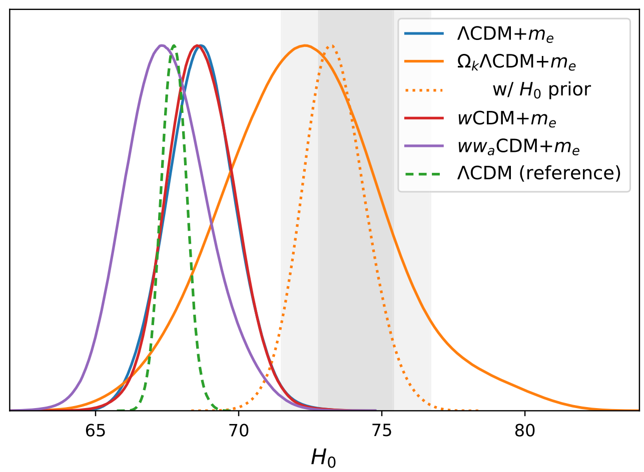


FIG. 3. Posterior distributions of $H_0$ for varying $m_e$ with different background models and the reference model. The gray band shows the direct $H_0$ measurement $H_0 = 74.1 \pm 1.3$ km/sec/Mpc without SNeIa [3]. Solid and dashed lines are obtained from the combination CMB + BAO + SNeIa. For ease of demonstration, we also depict the posterior distribution from CMB + BAO + SNeIa + H0 only for a varying-$m_e$ model with the $\Omega_k$ΛCDM background (orange dotted line).

(hereafter H0) [3],[7] which is not incorporated in the default parameter estimation.

From the figure, one can immediately see that the varying $m_e$ in the $\Omega_k$ΛCDM model gives a posterior distribution that matches well with the direct measurements. As expected

[7]This constraint is derived from direct measurements of $H_0$, including lens time decays [2], distances to water-maser galaxies from Ref. [29], and distance ladder measurements [30]. To minimize the influence of systematic errors associated with SNeIa, here we adopt results of distance ladder measurements without SNeIa.

TABLE I. Summary of parameter estimations of $m_e$ and $H_0$, and measures of the H0 tension, $\Delta\chi^2_{\rm eff}$, and $\log R$.

| | varying $m_e$ | | | | Constant $m_e$ |
|---|---|---|---|---|---|
| | $\Lambda$CDM | $\Omega_k\Lambda$CDM | $w$CDM | $ww_a$CDM | $\Lambda$CDM (reference) |
| $H_0$ [km/ sec /Mpc] (mean with 68% errors) | | | | | |
| based on CMB + BAO + SNeIa | $68.7^{+1.2}_{-1.2}$ | $72.3^{+2.7}_{-2.8}$ | $68.7^{+1.1}_{-1.2}$ | $67.5^{+1.3}_{-1.6}$ | $67.7^{+0.4}_{-0.4}$ |
| based on CMB + BAO + SNeIa + H0 | $71.1^{+0.9}_{-0.9}$ | $73.8^{+1.2}_{-1.2}$ | $71.0^{+0.9}_{-1.0}$ | $71.6^{+1.0}_{-1.0}$ | $68.4^{+0.4}_{-0.4}$ |
| $m_e/m_{e,0}$ (mean with 68% errors) | | | | | |
| based on CMB + BAO + SNeIa | $1.006^{+0.007}_{-0.007}$ | $1.052^{+0.030}_{-0.035}$ | $1.004^{+0.009}_{-0.010}$ | $0.992^{+0.012}_{-0.014}$ | … |
| based on CMB + BAO + SNeIa + H0 | $1.019^{+0.005}_{-0.005}$ | $1.068^{+0.016}_{-0.016}$ | $1.018^{+0.009}_{-0.009}$ | $1.026^{+0.012}_{-0.014}$ | … |
| $\Delta\chi^2_{\rm eff}$ relative to the reference | | | | | |
| based on CMB + BAO + SNeIa + H0 | −12.2 | −23.5 | −12.5 | −13.2 | 0 |
| $\log R$ | | | | | |
| based on CMB + BAO + SNeIa vs H0 | $-1.5 \pm 0.4$ | $1.9 \pm 0.4$ | $-1.2 \pm 0.4$ | $-1.2 \pm 0.4$ | $-7.5 \pm 0.4$ |
| PPD | | | | | |
| based on CMB + BAO + SNeIa vs H0 | $3.3\sigma$ | $2.2\sigma$ | $3.3\sigma$ | $3.2\sigma$ | $4.8\sigma$ |

from the parameter degeneracy discussed above, the $\Omega_k\Lambda$CDM background allows substantially broader distributions compared to the reference model.

Besides, it is remarkable that the distribution peak coincides with the direct $H_0$ measurements. The preference for higher $H_0$ in association with $\Omega_k < 0$ is brought about by the *Planck* data at $\ell > 30$, which is known to favor a larger lens amplitude, $A_{\rm L} > 1$ [4]. Indeed, we found that the posterior mean values in our analysis, which are consistent with local $H_0$ measurements, yield $C_\ell^{TT}$ at $\ell \gtrsim 800$, similar to that from the baseline but with $A_{\rm L} = 1.1$. Although a closed Universe enhances the CMB lensing effect and mitigates the lensing anomaly [31,32], in general the fit to BAO and SNeIa gets worse. However, varying $m_e$ in the $\Omega_k\Lambda$CDM model can maintain an excellent fit to BAO and SNeIa data.

While $H_0$ tension is relaxed with a varying $m_e$ in other backgrounds too, with the posterior distribution broadened from the reference model their peaks are still displaced from the direct measurements. In particular, allowing the DE EoS $w \neq -1$ hardly changes the situation, in contrast to the spatial curvature. This is because, being tightly constrained by BAO and SNeIa data, the DE EoS cannot significantly change $D_M(z_*)$. On the other hand, spatial curvature can change $D_M(z_*)$ without greatly affecting the low-$z$ distances.

Table I summarizes the mean values and 68% intervals of $H_0$ from the default data set (CMB + BAO + SNeIa) and an extended one (CMB+BAO+SNeIa+H0). For more detailed results of parameter estimation including constraints on other cosmological parameters, we refer readers to the Appendix A.

## VI. HOW MUCH IS THE $H_0$ TENSION RELAXED?

To assess how much the $H_0$ tension is relaxed in models we consider, we employ a few statistical measures: the relative effective chi square $\Delta\chi^2_{\rm eff}$, the Bayes ratio $R$, and the posterior predictive density (PPD). $R$ is defined as [33,34]

$$R = \frac{P(A,B|M)}{P(A|M)P(B|M)} = \frac{P(A|B,M)}{P(A|M)} = \frac{P(B|A,M)}{P(B|M)}, \tag{13}$$

where given a data set $A$ and a predictive model $M$, $P(A|M) = \int d\theta P(A|\theta)P(\theta|M)$ is the Bayes evidence, with $P(A|\theta)$ and $P(\theta|M)$ being the likelihood function and prior probability distribution of model parameters $\theta$ of $M$, respectively. $R$ gives the relative confidence of $A$ and $B$ and thus quantifies their compatibility. On the other hand, the PPD is defined as

$$\mathrm{PPD} = P(B|A,M), \tag{14}$$

which assumes that $A$ is the data, with which we infer the posterior distribution, and $B$ is the holdout data for validation. The PPD can be translated into an equivalent $\sigma$ value. We refer readers to Appendix B for the advantages and disadvantages of $R$ and the PPD.

For our purpose of quantifying the $H_0$ tension, we adopt the combination CMB + BAO + SNeIa as $A$ and H0 as $B$. Bayesian evidence is computed using CosmoChord [35]. Table I lists the $\log R$ and PPD for each model as well as $\Delta\chi^2$ from the reference model ($\Lambda$CDM without a varying $m_e$). The reference model gives a large negative $\log R = -7.5$ and a $4.8\sigma$ deviation in the PPD, which manifests the severity of the $H_0$ tension. In contrast, the varying-$m_e$ model in $\Omega_k\Lambda$CDM gives a positive $\log R = 1.9$ and only a $2.2\sigma$ deviation in the PPD with $\Delta\chi^2_{\rm eff} = -23.5$ from the reference model. These results prove that data strongly prefers a varying $m_e$ in $\Omega_k\Lambda$CDM, which can resolve the $H_0$ tension, over the reference model. In other varying-$m_e$ models, the tension is significantly moderated but is not completely resolved.

## VII. CONCLUSION

It has been very difficult to reduce the scale of the sound horizon on the last scattering surface, which is key to solving the Hubble tension. In the framework of modified recombination, we have discussed general conditions that successful models should satisfy. Moreover, we have also presented a model with a varying $m_e$ as an excellent working example. With a positive spatial curvature of the Universe, the varying-$m_e$ model can fit not only CMB but also low-$z$ distances such as BAO and SNeIa simultaneously. Remarkably, once fitted to those cosmological data, the model *predicts* a high $H_0$ perfectly consistent with direct measurements, which makes the model quite distinct from other solutions proposed in the literature.

The parameter degeneracy in Eq. (4) is not perfect, and a varying $m_e$ distorts CMB power spectra through the non-equilibrium nature of recombination. Therefore, CMB-S4 [36] may be able to constrain/verify our examples. Substantial deviations from the baseline at low-$z$ distances are also predicted. For instance, when varying $m_e$ with $\Omega_k\Lambda$CDM background, $\Delta_{r_s(z_{\rm drag})} \simeq -0.05$ and $\Omega_k \simeq -0.01$ are required to solve the $H_0$ tension. Future distance measurements will be able to test such deviations from the baseline [37].

## ACKNOWLEDGMENTS

This work is supported by JSPS KAKENHI Grants No. 18H04339 (T. S.), No. 18K03640 (T. S.), No. 17H01131 (T. T., T. S.), No. 19K03874 (T. T.), and MEXT KAKENHI Grant No. 19H05110 (T. T.). This research was conducted using the Fujitsu PRIMERGY CX600M1/CX1640M1 (Oakforest-PACS) in the Information Technology Center, The University of Tokyo.

## APPENDIX A: PARAMETER ESTIMATION

We summarize the one-dimensional marginalized posterior mean and 68% intervals of relevant cosmological parameters in Tables II–VI and their triangle plots in Figs. 4–8.

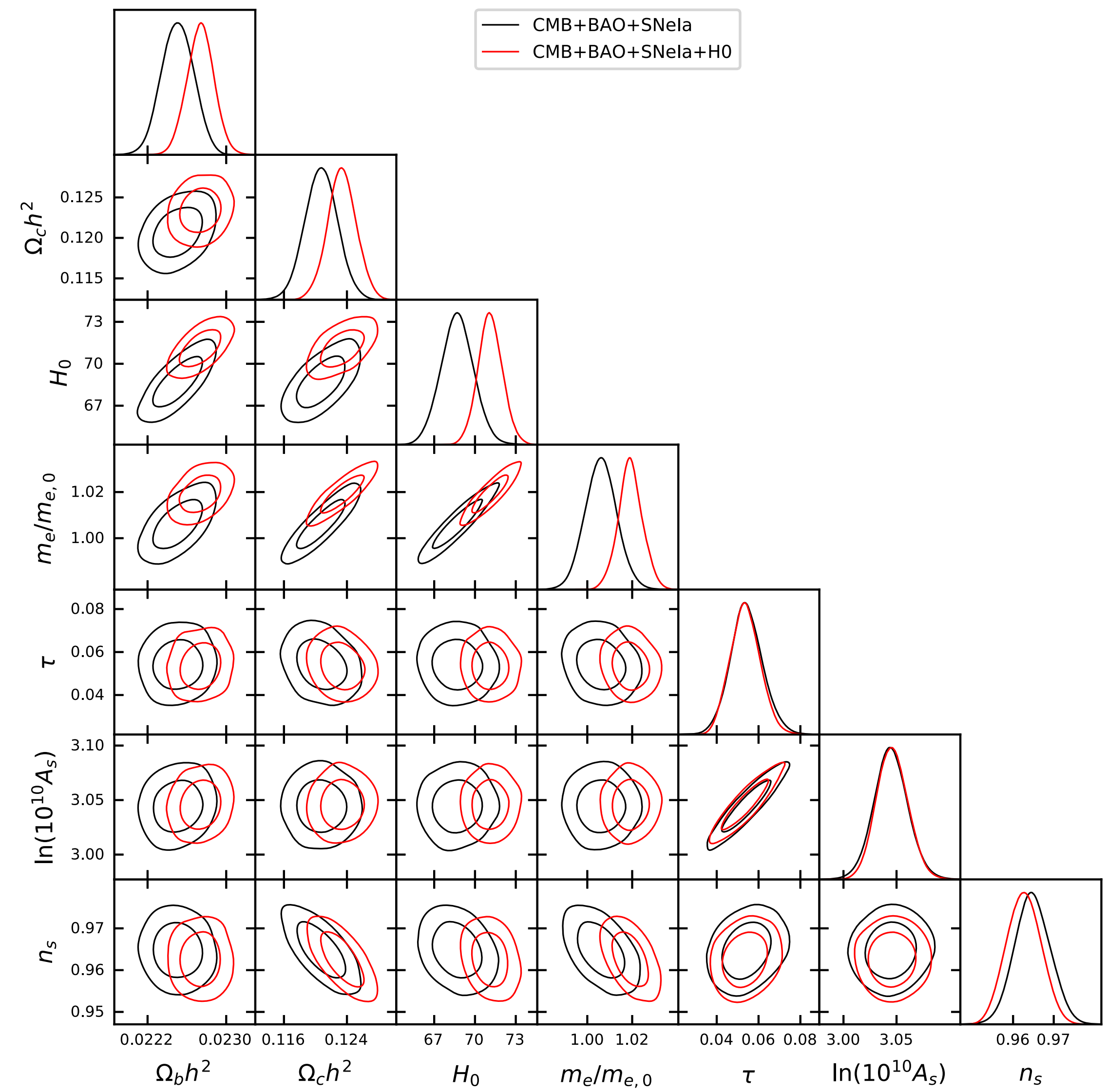


FIG. 4. Two-dimensional constraints in the ΛCDM model with a varying $m_e$.

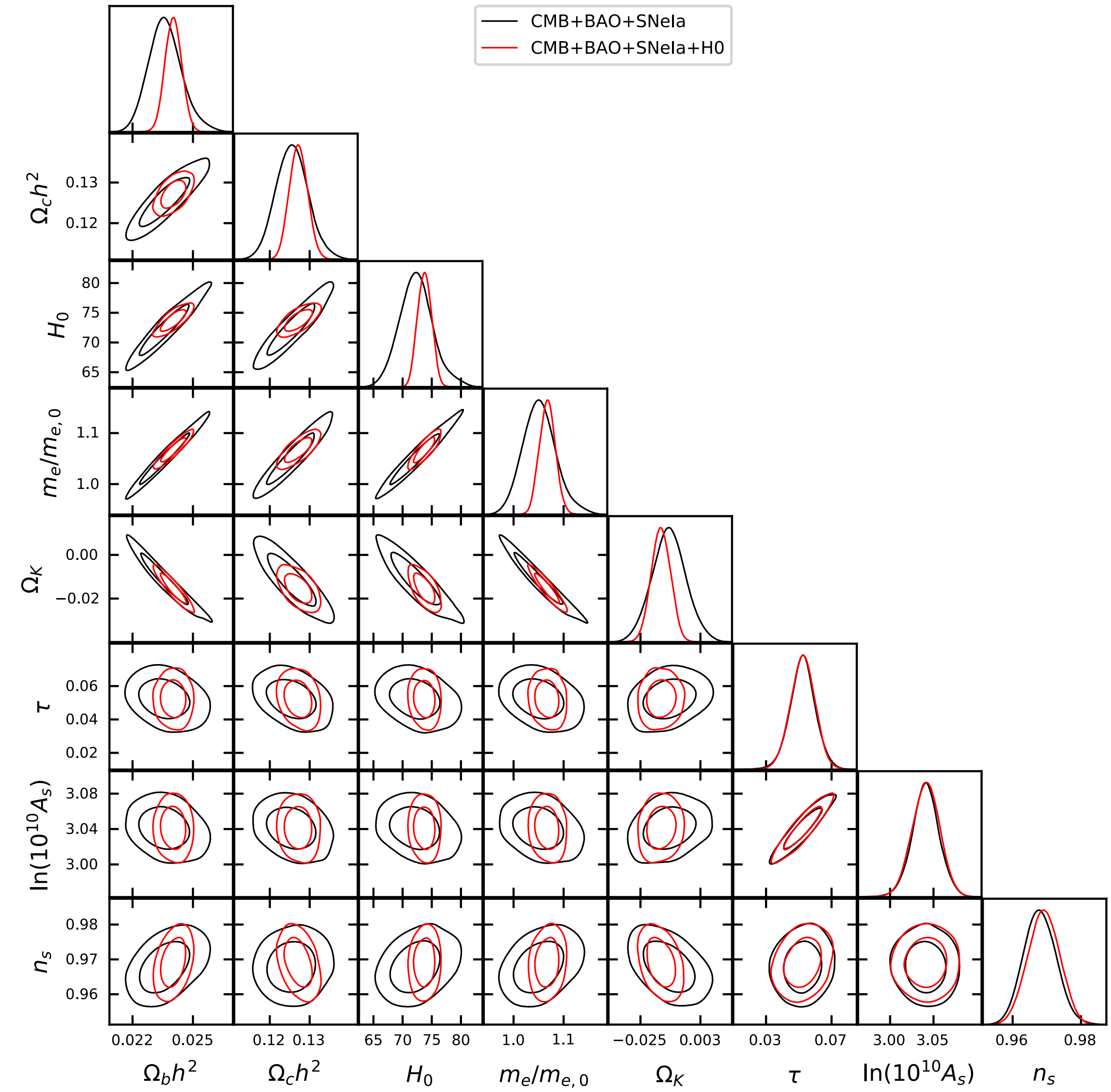


FIG. 5. Same as in Fig. 4 but in the $\Omega_k\Lambda$CDM model with a varying $m_e$.

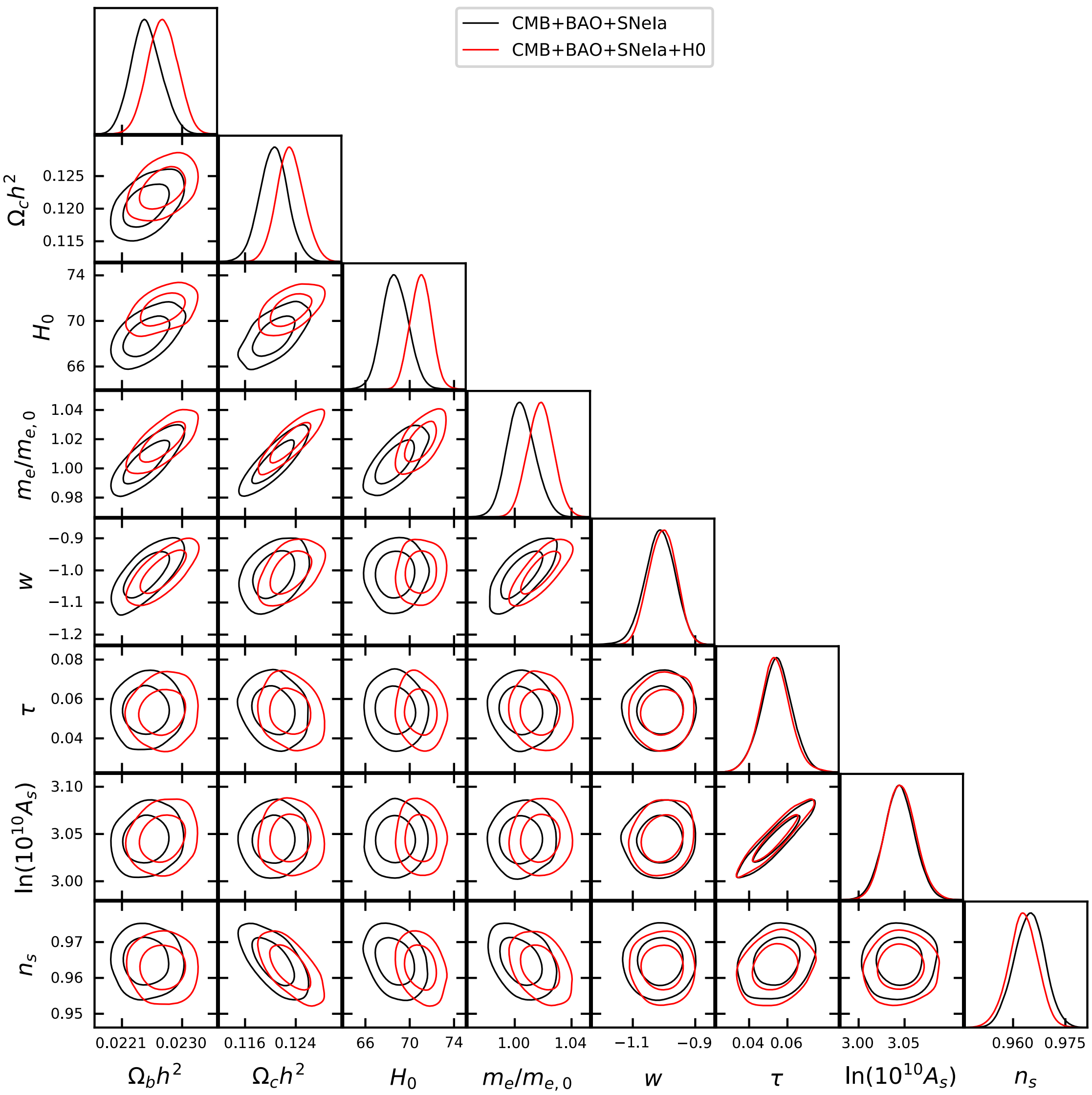


FIG. 6. Same as in Fig. 4 but in the $w$CDM model with a varying $m_e$.

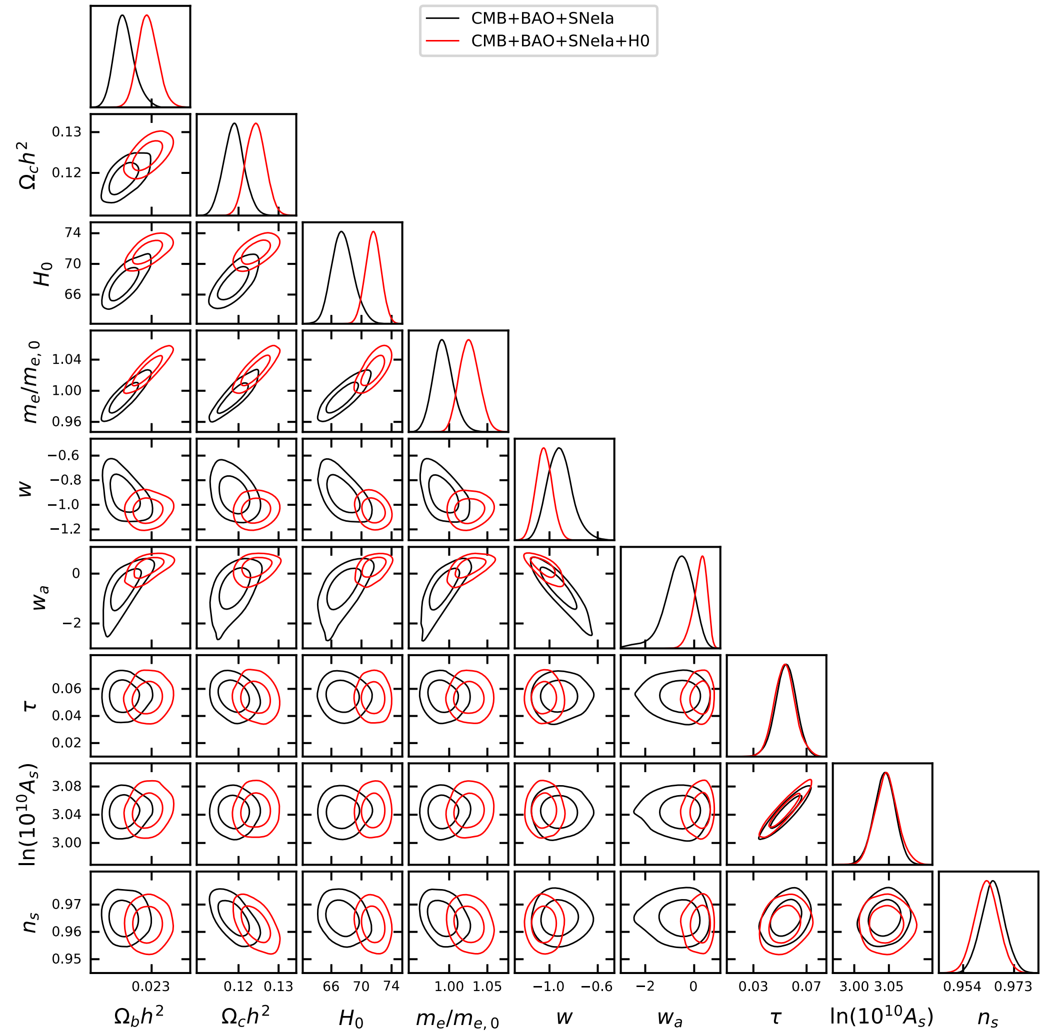


FIG. 7. Same as in Fig. 4 but in the $ww_a$CDM model with a varying $m_e$.

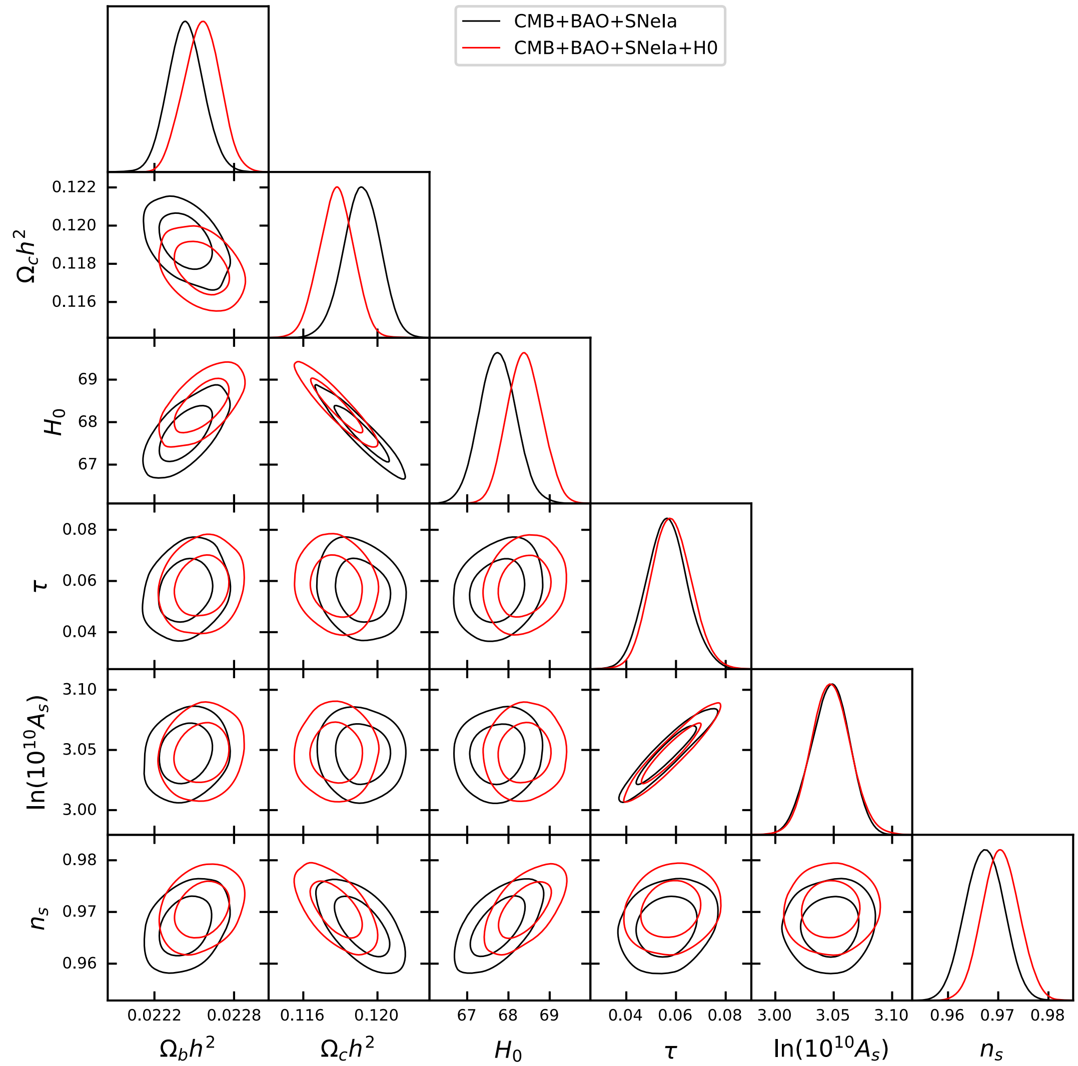


FIG. 8. Same as in Fig. 4 but in the reference ΛCDM model with a constant $m_e$.

TABLE II. Parameter estimation in $m_e\Lambda$CDM.

| | CMB + BAO+ SNeIa | CMB + BAO+ SNeIa + H0 |
|---|---|---|
| $100\omega_b$ | $2.251^{+0.016}_{-0.016}$ | $2.274^{+0.013}_{-0.014}$ |
| $\omega_c$ | $0.1207^{+0.002}_{-0.0021}$ | $0.1234^{+0.0018}_{-0.0017}$ |
| $\theta$ | $1.0452^{+0.0049}_{-0.0049}$ | $1.0545^{+0.0037}_{-0.0036}$ |
| $\tau_{\rm reion}$ | $0.0543^{+0.0073}_{-0.008}$ | $0.0537^{+0.0071}_{-0.0072}$ |
| $\log(10^{10}A_s)$ | $3.045^{+0.016}_{-0.016}$ | $3.046^{+0.014}_{-0.015}$ |
| $n_s$ | $0.9648^{+0.0045}_{-0.0043}$ | $0.9626^{+0.0043}_{-0.0043}$ |
| $m_e/m_{e,0}$ | $1.0061^{+0.0069}_{-0.007}$ | $1.0192^{+0.0052}_{-0.0055}$ |
| $H_0$ [km/ sec /Mpc] | $68.7^{+1.2}_{-1.2}$ | $71.12^{+0.87}_{-0.86}$ |
| $r_s(z_{\rm drag})$ [Mpc] | $146.2^{+1.2}_{-1.2}$ | $144.12^{+0.89}_{-0.94}$ |

TABLE III. Parameter estimation in $m_e\Omega_k\Lambda$CDM.

| | CMB + BAO +SNeIa | CMB + BAO+ SNeIa + H0 |
|---|---|---|
| $100\omega_b$ | $2.363^{+0.074}_{-0.088}$ | $2.403^{+0.041}_{-0.041}$ |
| $\omega_c$ | $0.1256^{+0.0039}_{-0.0041}$ | $0.1272^{+0.0023}_{-0.0023}$ |
| $\theta$ | $1.077^{+0.022}_{-0.023}$ | $1.088^{+0.011}_{-0.011}$ |
| $\tau_{\rm reion}$ | $0.0523^{+0.0075}_{-0.0075}$ | $0.0523^{+0.0075}_{-0.0075}$ |
| $\log(10^{10}A_s)$ | $3.041^{+0.015}_{-0.015}$ | $3.041^{+0.016}_{-0.016}$ |
| $n_s$ | $0.968^{+0.0048}_{-0.0047}$ | $0.9691^{+0.0047}_{-0.0046}$ |
| $m_e/m_{e,0}$ | $1.052^{+0.03}_{-0.035}$ | $1.068^{+0.016}_{-0.016}$ |
| $\Omega_k$ | $-0.0117^{+0.0079}_{-0.0081}$ | $-0.0154^{+0.0046}_{-0.0045}$ |
| $H_0$ [km/ sec /Mpc] | $72.3^{+2.7}_{-2.8}$ | $73.8^{+1.2}_{-1.2}$ |
| $r_s(z_{\rm drag})$ [Mpc] | $140^{+4.5}_{-4.3}$ | $137.9^{+2.1}_{-2}$ |

TABLE IV. Parameter estimation in $m_e w$CDM.

| | CMB + BAO+ SNeIa | CMB + BAO+ SNeIa + H0 |
|---|---|---|
| $\omega_b$ | $2.246^{+0.021}_{-0.024}$ | $2.271^{+0.023}_{-0.022}$ |
| $\omega_c$ | $0.1205^{+0.0021}_{-0.0022}$ | $0.1232^{+0.002}_{-0.0022}$ |
| $\theta$ | $1.0441^{+0.0065}_{-0.0073}$ | $1.0537^{+0.0062}_{-0.0066}$ |
| $\tau_{\rm reion}$ | $0.0543^{+0.0078}_{-0.0079}$ | $0.0535^{+0.0075}_{-0.0074}$ |
| $\log(10^{10}A_s)$ | $3.044^{+0.016}_{-0.016}$ | $3.046^{+0.016}_{-0.017}$ |
| $n_s$ | $0.9647^{+0.0043}_{-0.0043}$ | $0.9629^{+0.0042}_{-0.004}$ |
| $m_e/m_{e,0}$ | $1.0045^{+0.0091}_{-0.01}$ | $1.0182^{+0.0089}_{-0.0094}$ |
| $w$ | $-1.013^{+0.048}_{-0.046}$ | $-1.005^{+0.044}_{-0.045}$ |
| $H_0$ [km/ sec /Mpc] | $68.7^{+1.1}_{-1.2}$ | $71.01^{+0.94}_{-0.99}$ |
| $r_s(z_{\rm drag})$ [Mpc] | $146.5^{+1.6}_{-1.5}$ | $144.3^{+1.5}_{-1.5}$ |

TABLE V. Parameter estimation in $m_e w w_a$CDM.

| | CMB + BAO+ SNeIa | CMB + BAO+ SNeIa + H0 |
|---|---|---|
| $100\omega_b$ | $2.221^{+0.024}_{-0.032}$ | $2.289^{+0.026}_{-0.03}$ |
| $\omega_c$ | $0.1189^{+0.0024}_{-0.0025}$ | $0.1243^{+0.0024}_{-0.0024}$ |
| $\theta$ | $1.0353^{+0.0084}_{-0.0099}$ | $1.0595^{+0.0085}_{-0.0095}$ |
| $\tau_{\rm reion}$ | $0.0545^{+0.0076}_{-0.0075}$ | $0.0535^{+0.0075}_{-0.0079}$ |
| $\log(10^{10}A_s)$ | $3.044^{+0.015}_{-0.015}$ | $3.046^{+0.016}_{-0.016}$ |
| $n_s$ | $0.9651^{+0.0042}_{-0.0043}$ | $0.9627^{+0.0044}_{-0.0044}$ |
| $m_e/m_{e,0}$ | $0.992^{+0.012}_{-0.014}$ | $1.026^{+0.012}_{-0.014}$ |
| $w$ | $-0.914^{+0.09}_{-0.11}$ | $-1.045^{+0.067}_{-0.067}$ |
| $w_a$ | $-0.64^{+0.65}_{-0.44}$ | $0.24^{+0.33}_{-0.2}$ |
| $H_0$ [km/ sec /Mpc] | $67.5^{+1.3}_{-1.6}$ | $71.6^{+1}_{-1}$ |
| $r_s(z_{\rm drag})$ [Mpc] | $148.3^{+2.1}_{-2}$ | $143.1^{+2}_{-1.8}$ |

TABLE VI. Parameter estimation in ΛCDM (constant $m_e$).

| | CMB + BAO+ SNeIa | CMB + BAO+ SNeIa + H0 |
|---|---|---|
| $\omega_b$ | $2.244^{+0.013}_{-0.013}$ | $2.256^{+0.014}_{-0.014}$ |
| $\omega_c$ | $0.11916^{+0.00096}_{-0.00097}$ | $0.11779^{+0.00093}_{-0.00092}$ |
| $\theta$ | $1.04103^{+0.0003}_{-0.00027}$ | $1.04119^{+0.00028}_{-0.00029}$ |
| $\tau_{\rm reion}$ | $0.0564^{+0.0078}_{-0.0081}$ | $0.0581^{+0.0076}_{-0.0083}$ |
| $\log(10^{10}A_s)$ | $3.047^{+0.017}_{-0.016}$ | $3.048^{+0.016}_{-0.016}$ |
| $n_s$ | $0.9673^{+0.0038}_{-0.0038}$ | $0.9705^{+0.0036}_{-0.0037}$ |
| $H_0$ [km/ sec /Mpc] | $67.74^{+0.43}_{-0.44}$ | $68.39^{+0.42}_{-0.42}$ |
| $r_s(z_{\rm drag})$ [Mpc] | $147.24^{+0.23}_{-0.25}$ | $147.47^{+0.24}_{-0.23}$ |

## APPENDIX B: BAYES RATIO AND POSTERIOR PREDICTIVE DISTRIBUTION

Here we describe our Bayesian measures of tension between two data sets: the Bayes ratio and posterior predictive distribution. Provided data $D$ and predictive model $M$ with model parameter $\theta$, the Bayes theorem gives the relation between the input and output in Bayesian statistical inference:

$$P(\theta|D,M)P(D|M) = P(D|\theta,M)P(\theta|M), \tag{B1}$$

where $P(\theta|D,M)$ is the posterior probability distribution,

$$P(D|M) = \int P(D|\theta,M)P(\theta|M)d\theta \tag{B2}$$

is the Bayes evidence, $P(D|\theta,M)$ is the likelihood function, and $P(\theta|M)$ is the prior probability function.

Given two data sets $A$ and $B$, one may regard $A$ as training data and $B$ as the holdout data for validation. Then, the PPD can be defined as

$$\begin{aligned} P(B|A,M) &= \int P(B|\theta,M)P(\theta|A,M)d\theta \\ &= \frac{P(A,B|M)}{P(A|M)}. \end{aligned} \tag{B3}$$

One of the advantage of using the PPD is that, since it is a probability distribution, it can be translated into an equivalent $\sigma$ value and easily interpreted. In addition, when $A$ is constraining enough, the PPD depends very weakly on the prior distribution. On the other hand, it is not symmetric under the exchange of $A$ and $B$, and hence an arbitrariness arises from the choice of training and holdout data sets.

On the other hand, the Bayes ratio is defined as

$$\begin{aligned} R &\equiv \frac{P(A,B|M)}{P(A|M)P(B|M)} \\ &= \frac{P(A|B,M)}{P(A|M)} \\ &= \frac{P(B|A,M)}{P(B|M)}. \end{aligned} \tag{B4}$$

From the second and third lines, one can immediately see that the Bayes ratio gives the relative confidence of different data sets. When posterior distributions $P(\theta|A,M)$ and $P(\theta|B,M)$ in the parameter space of $\theta$ overlap with each other, $R$ becomes large. Oppositely, when $P(\theta|A,M)$ and $P(\theta|B,M)$ are displaced, $R$ becomes small. Therefore, $R$ measures the compatibility of $A$ and $B$. In general, $R$ depends on the prior distribution, while it is symmetric under the exchange of $A$ and $B$.

In our case, $A$ is the combination CMB + BAO + SNeIa and $B$ is $H0$. In Table VII we summarize the values of the

TABLE VII. Summary of Bayes evidence.

| | CMB + BAO + SNeIa | H0 | CMB + BAO + SNeIa + H0 |
|---|---|---|---|
| varying $m_e$ | | | |
| $\Lambda$CDM | $-1952.5 \pm 0.3$ | $-3.11 \pm 0.07$ | $-1957.1 \pm 0.3$ |
| $\Omega_k\Lambda$CDM | $-1952.6 \pm 0.3$ | $-3.45 \pm 0.07$ | $-1954.1 \pm 0.3$ |
| $w$CDM | $-1955.3 \pm 0.3$ | $-3.29 \pm 0.07$ | $-1959.9 \pm 0.3$ |
| $ww_a$CDM | $-1957.0 \pm 0.3$ | $-3.11 \pm 0.07$ | $-1961.3 \pm 0.3$ |
| const $m_e$ | | | |
| $\Lambda$CDM (ref) | $-1949.3 \pm 0.3$ | $-3.17 \pm 0.07$ | $-1960.0 \pm 0.3$ |

Bayes evidence $R$ and our measures of the tension PPD. As one can see in Table VII, the Bayes evidence $P(B|M)$ is almost model independent, which is because all of the model parameters other than $H_0$ are entirely unconstrained. Therefore, the PPD and $R$ are accidentally almost proportional to one another in our case.

[1] A. G. Riess, S. Casertano, W. Yuan, L. M. Macri, and D. Scolnic, Astrophys. J. **876**, 85 (2019).
[2] K. C. Wong *et al.*, Mon. Not. R. Astron. Soc. **498**, 1420 (2020).
[3] A. G. Riess, Nat. Rev. Phys. **2**, 10 (2020).
[4] N. Aghanim *et al.* (Planck Collaboration), Astron. Astrophys. **641**, A6 (2020).
[5] E. Aubourg *et al.*, Phys. Rev. D **92**, 123516 (2015).
[6] J. L. Bernal, L. Verde, and A. G. Riess, J. Cosmol. Astropart. Phys. 10 (2016) 019.
[7] E. Mörtsell and S. Dhawan, J. Cosmol. Astropart. Phys. 09 (2018) 025.
[8] K. Aylor, M. Joy, L. Knox, M. Millea, S. Raghunathan, and W. K. Wu, Astrophys. J. **874**, 4 (2019).
[9] L. Knox and M. Millea, Phys. Rev. D **101**, 043533 (2020).
[10] C.-T. Chiang and A. Z. Slosar, arXiv:1811.03624.
[11] M. Liu, Z. Huang, X. Luo, H. Miao, N. K. Singh, and L. Huang, Sci. China Phys. Mech. Astron. **63**, 290405 (2020).
[12] J. D. Barrow and J. Magueijo, Phys. Rev. D **72**, 043521 (2005).
[13] J. D. Barrow, Phys. Rev. D **71**, 083520 (2005).
[14] C. Martins, arXiv:1709.02923.
[15] L. Hart and J. Chluba, Mon. Not. R. Astron. Soc. **493**, 3255 (2020).
[16] P. Ade *et al.* (Planck Collaboration), Astron. Astrophys. **580**, A22 (2015).
[17] L. Hart and J. Chluba, Mon. Not. R. Astron. Soc. **474**, 1850 (2018).
[18] A. Lewis, A. Challinor, and A. Lasenby, Astrophys. J. **538**, 473 (2000).
[19] Y. Ali-Haimoud and C. M. Hirata, Phys. Rev. D **83**, 043513 (2011).
[20] F. Beutler, C. Blake, M. Colless, D. Jones, L. Staveley-Smith, L. Campbell, Q. Parker, W. Saunders, and F. Watson, Mon. Not. R. Astron. Soc. **416**, 3017 (2011).
[21] A. J. Ross, L. Samushia, C. Howlett, W. J. Percival, A. Burden, and M. Manera, Mon. Not. R. Astron. Soc. **449**, 835 (2015).
[22] S. Alam *et al.* (BOSS Collaboration), Mon. Not. R. Astron. Soc. **470**, 2617 (2017).
[23] D. Scolnic *et al.*, Astrophys. J. **859**, 101 (2018).
[24] A. Lewis and S. Bridle, Phys. Rev. D **66**, 103511 (2002).
[25] N. Aghanim *et al.* (Planck Collaboration), Astron. Astrophys. **641**, A5 (2020).
[26] J. Chluba and R. Thomas, Mon. Not. R. Astron. Soc. **412**, 748 (2011).
[27] M. Chevallier and D. Polarski, Int. J. Mod. Phys. D **10**, 213 (2001).
[28] E. V. Linder, Phys. Rev. Lett. **90**, 091301 (2003).
[29] D. Pesce *et al.*, Astrophys. J. Lett. **891**, L1 (2020).
[30] M. Reid, D. Pesce, and A. Riess, Astrophys. J. Lett. **886**, L27 (2019).
[31] W. Handley, Phys. Rev. D **103**, L041301 (2021).
[32] E. Di Valentino, A. Melchiorri, and J. Silk, Nat. Astron. **4**, 196 (2020).
[33] P. Marshall, N. Rajguru, and A. Slosar, Phys. Rev. D **73**, 067302 (2006).
[34] F. Feroz, B. C. Allanach, M. Hobson, S. S. AbdusSalam, R. Trotta, and A. M. Weber, J. High Energy Phys. 10 (2008) 064.
[35] W. Handley, M. Hobson, and A. Lasenby, Mon. Not. R. Astron. Soc. **453**, 4385 (2015).
[36] K. N. Abazajian *et al.* (CMB-S4 Collaboration), arXiv:1610.02743.
[37] M. Denissenya, E. V. Linder, and A. Shafieloo, J. Cosmol. Astropart. Phys. 03 (2018) 041.